Acta Materialia 113 (2016) 272–283

Contents lists available at ScienceDirect

Acta Materialia

journal homepage: www.elsevier.com/locate/actamat

Full length article

Hydrogen assisted crack initiation and propagation in a nickel-based superalloy

Zhenbo Zhang [a, *], Gideon Obasi [a], Roberto Morana [b], Michael Preuss [a]

[a] BP International Centre for Advanced Materials, School of Materials, University of Manchester, M13 9PL, UK
[b] BP Exploration Operating Company Limited, Chertsey Road, Sunbury-on-Thames, TW16 7LN, UK

ARTICLE INFO

Article history:
Received 27 February 2016
Received in revised form
28 April 2016
Accepted 1 May 2016
Available online 14 May 2016

Keywords:
Nickel-based superalloy
Hydrogen embrittlement
Electron channeling contrast imaging
Slip localisation
Quasi-cleavage fracture

ABSTRACT

To understand the mechanism for hydrogen-induced embrittlement in a nickel-based superalloy, detailed electronmicroscopy characterisation has been employed on the UNS N07718 (Alloy 718) after hydrogen charging and slow strain rate testing to investigate the strain localisation and damage accumulation caused by hydrogen. Transmission Electron Microscopy analysis demonstrates that the microstructure of the material after tension is characterised by planar dislocation slip bands (DSBs) along {111}γ planes. Consistent results from Electron Channeling Contrast Imaging (ECCI) reveal that cracks always propagate along planar DSBs in the presence of hydrogen. This phenomenon is rationalized by the evident nucleation of nanoscale voids along the DSBs, especially at the intersections between nonparallel DSBs. The proposed mechanism, confirmed by both the ECCI analysis and fractographic study by Scanning Electron Microscopy, indicates that the interaction between the hydrogen and dislocations along the DSBs leads to void nucleation. Furthermore, the results suggest that coalescence and widening of voids via the dislocation process promote the crack propagation along the DSBs in hydrogen charged Alloy 718.

1. Introduction

Structural materials used in the oil and gas deep wells face extremely aggressive environments, including low pH (H_2S), high temperature (>250 °C) and high pressure (>100 MPa) [1,2]. High strength nickel-based superalloys are promising structural materials for application in these challenging conditions, because of their capability to operate at the high temperature and high pressure conditions providing outstanding corrosion resistance. One longstanding challenge, however, is the hydrogen-induced embrittlement when these alloys are exposed to hydrogenating conditions such as the sour environments of deep wells: adsorption of hydrogen leads to changes in the fracture mode of nickel-based superalloys from ductile to brittle [3–6].

A number of mechanisms have been proposed to account for the hydrogen embrittlement in various materials under different hydrogen charging conditions [7–14]. For the metallic materials that do not form hydrides, such as Fe and Ni, the most commonly invoked embrittlement mechanisms are hydrogen-enhanced decohesion (HEDE) [12,13] and hydrogen-enhanced localised plasticity (HELP) [8,9]. According to the HEDE mechanism, the hydrogen can reduce the cohesive strength of the atomic bonding. Consequently, grain boundaries and precipitate/matrix interfaces that accumulate hydrogen beyond a critical concentration will fracture when the material is stressed. The HEDE mechanism was raised to interpret the load relaxation and intergranular failure caused by hydrogen. Although atomic scale simulations [15–17] support it, the lack of direct experimental evidence places some doubt on the relevance of this mechanism. The HELP mechanism was first suggested by Beachem [8], and was then underpinned by in-situ transmission electron microscopy (TEM) analysis, where the mobility of dislocations was evidently enhanced by the presence of hydrogen [9]. The theoretical basis for the HELP mechanism was rationalized by the hydrogen shielding effect on dislocations [18,19]. In this framework, the dislocation slip mode and dislocation-dislocation interaction are modified and specifically the equilibrium distance between dislocations is decreased [20,21]. Furthermore, dislocation slip planarity is promoted due to the dragging of hydrogen [19]. Accordingly, extensive dislocation slip is expected, and dislocation motion and dislocation-dislocation interaction are largely constrained to the initial slip plane due to limited cross slip in the presence of hydrogen.

* Corresponding author.
E-mail addresses: zhenbo.zhang@manchester.ac.uk, zbzhang85@gmail.com (Z. Zhang).

http://dx.doi.org/10.1016/j.actamat.2016.05.003
1359-6454/

Phenomenologically, hydrogen embrittlement in metallic materials is generally characterised by intergranular cracking with quasi-cleavage fracture surface. Experimental studies have demonstrated that extensive dislocation activities and plasticity are associated with hydrogen embrittlement [11,22–27]. Martin et al. studied the microstructure beneath the quasi-cleavage fracture surface of a ferritic steel [22,23] and pure Ni [24], and found a good correlation between the features on the fracture surface and the underneath dislocation substructure, which indicates the importance of dislocation activities on the hydrogen embrittlement. More importantly, they flagged up that the dislocation substructure in the hydrogen containing material is finer than in the one without hydrogen [24,27,28], which provides further support for the HELP mechanism. Besides the HEDE and HELP mechanisms, the hydrogen enhanced vacancy stabilization mechanism has also been proposed [10,11,29]. In this mechanism, hydrogen is supposed to stabilize vacancies generated by the dislocation activities and promote the formation of voids by the vacancy agglomeration [29]. Although the central aspect of this mechanism is different from that of the HELP mechanism, conceptually, in both cases hydrogen induced fracture originates from, and is promoted by, dislocation activities and therefore the crack nucleation is associated with the regions of extensive dislocation slip activities.

To date, most studies dedicated to understand the mechanism of hydrogen embrittlement of non-hydride forming metallic materials have been conducted on pure nickel [9,24,30] and some steels [22,25–27,31–33]. For nickel-based superalloys, investigations have mainly focused on the fracture mode and the effect of different heat treatments on mechanical properties in regard to hydrogen embrittlement [3–5,34–37]. Since in precipitation-hardened nickel-based superalloys the interfaces between the precipitates (γ', γ'', δ and carbides) and γ matrix are often assumed to be the trapping sites for hydrogen, studies have focused on modifying the size and volume fraction of the various precipitates by specific heat treatments and compare hydrogen embrittlement susceptibility of the resulting microstructures [4,5,36,37]. Even though the activity of dislocations is demonstrated to be of crucial importance for hydrogen embrittlement in several materials, to the authors' knowledge, there is no work carried out to clarify the mechanism on this aspect in nickel-based superalloys.

In the present study, hydrogen-induced embrittlement was studied for the precipitation-hardened nickel-based superalloy UNS N07718 (Alloy 718), which is a widely used structural material for deep well application in the oil and gas industry. The correlation between the microstructural features, especially the dislocation substructure developed during straining, and the crack initiation and propagation was explored in detail by extensive Scanning Electron Microscopy (SEM), high resolution Electron Channeling Contrast Imaging (ECCI), Electron Backscattered Diffraction (EBSD) and TEM characterisations. The observations are discussed in context of previous studies related to hydrogen-induced embrittlement and a mechanistic framework is proposed for precipitation-hardened nickel-based superalloys involving dislocation slip localisation in conjunction with hydrogen promoting vacancy production.

2. Experimental

Cylindrical blanks with a diameter of 8 mm and a length of 60 mm were machined from the Alloy 718 ingot (commercially heat-treated to aerospace specifications) and solution treated at 1040 °C for 1 h followed by the furnace cooling (cooling rate is approximately 15 °C/min). The material was subsequently aged at 774 °C for 6 h followed by cooling in air. To minimise the surface oxidation, all heat treatments were carried out in an argon atmosphere. The purpose of this heat treatment was to generate a condition that is more typical for oil and gas applications.

Tensile samples with a gauge length of 25.0 mm and a diameter of 3.8 mm were machined from the heat-treated cylinders by means of electro discharge machining (EDM). The machined samples were then ground with fine silicon carbide paper to remove the recast layer from the EDM process.

Cathodic hydrogen charging was conducted at 80 °C in a NaCl (1 mol/L) solution. The samples were charged with a constant electric current density of 7.7 mA/cm^2 for 168 h. The penetration depth of the hydrogen can be estimated according to the diffusion equation:

$$x = \sqrt{2Dt} \tag{1}$$

here, t is the charging time, and x is the penetration depth and D is the diffusion coefficient of hydrogen in Alloy 718. D can be calculated based on the equation [38]:

$$D = 4.06 \times 10^{-7} e^{\left(\frac{-48.63\times10^3}{RT}\right)} \tag{2}$$

here, R is the gas constant and T is the charging temperature, i.e. 353 K in the present case. Accordingly, the hydrogen penetration depth in the sample after charging for 168 h is estimated to be ~140 μm.

Both the charged and non-charged samples were slow strain rate (SSR) tested in tension with initial strain rate of 10^{-6} s^{-1} at the room temperature using an Instron machine with a 50 kN load cell. An extensometer was employed to measure the instant strain of the sample during tensioning. The fracture surface of the sample after failure was characterised using a Zeiss EVO60 SEM operating at 20 kV.

A FEI Magellan 400 field emission gun SEM equipped with a concentric backscatter electron detector was employed, which provides ideal imaging conditions for the ECCI analysis with very high resolution and excellent contrast. The gauge section of the hydrogen charged sample strained to failure was mid-sectioned longitudinally, followed by careful grinding and polishing. The sample for ECCI analysis was finished by polishing with 40 nm colloidal silica suspension (OPS, Struers). ECC imaging was conducted on the regions both close to the sample surface (where hydrogen had diffused to) and the sample interior (where hydrogen had not enough time to diffuse to), with a low accelerating voltage (3 kV–5 kV) and a short working distance in the range of 3.5–4 mm to enable a high resolution. EBSD analysis was performed using a FEI Quanta650 field emission gun SEM equipped with a HKL system operating at 20 kV. Orientation maps from the samples were obtained prior to and after the tensile testing. In addition, Kernel average misorientation (KAM) maps, i.e. average misorientation between the each data point and its nearest neighbours, were computed from the EBSD data of the sample after tensioning.

A FEI Tecnai G20 TEM operating at 200 kV was used to characterise the γ' distribution in the initial material and the dislocation substructure after the tension experiment (from the region without hydrogen). TEM foils were prepared by twin-jet electropolishing (TENUPOL5, Struers), in a solution of 10% perchloric acid and 90% methanol at a temperature of −35 °C.

3. Results

The initial microstructure of Alloy 718 after the heat treatment described above is shown in Fig. 1. The grain morphology, which was mapped out by EBSD, indicates an average grain size of about

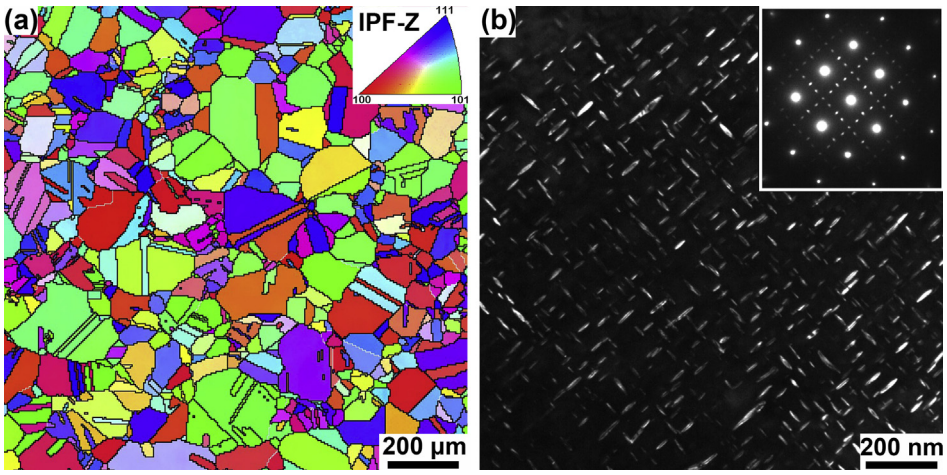

Fig. 1. Microstructure of the Alloy 718 prior to hydrogen charging and tension: (a) an orientation map obtained by EBSD, with color code shown in the inset; (b) a dark field TEM image showing the γ' with the incident electron beam along ⟨100⟩ zone axis of γ, and a corresponding selective area diffraction pattern in the inset. (For interpretation of the references to colour in this figure legend, the reader is referred to the web version of this article.)

62 μm with a $\sum$3 twin boundary (TB) fraction of 44% (see Fig. 1a). A dark field TEM image with the incident electron beam along the ⟨100⟩γ zone axis shows the needle-shaped γ' with a mean length of 23.5 nm (see Fig. 1b).

The stress-strain curves of the material, following the SSR tests with and without hydrogen charging, are shown in Fig. 2. It is found that the applied hydrogen charging has no appreciable effect on the yield stress, however, the total elongation decreases dramatically from 25% to about 12%. It is also worth noting that the work hardening rate of the hydrogen charged sample is lower than that of the non-charged sample. Fig. 2 includes a schematic illustrating the regions that were characterised in detail following the SSR experiment. Fig. 3 shows the fractographs obtained by SEM and the analysis demonstrates a multimode failure: brittle fracture features close to the sample surface (~200 μm to the sample outer surface), typical ductile failure in the sample interior and a transitional region with mixed failure mode in-between. The brittle fracture surface is typically fairly flat, and some traces and voids can be clearly seen in the high resolution image (Fig. 3b); overall this morphology is very different from the dimple containing structure observed in the ductile failure region (Fig. 3c).

Since the deformation microstructure developed during straining is believed to be crucial for understanding the material failure mechanism, a detailed microstructural characterisation was carried out on the hydrogen charged specimens, following the SSR test. As hydrogen only diffused into the outer rim of the sample, it was possible to study regions where hydrogen was present and regions that had not been affected by hydrogen on the same sample, and results are shown in Figs. 4 and 5. TEM analysis in Fig. 4a, performed at the sample interior (no diffused hydrogen), shows planar dislocation boundaries. An ECCI image from the specimen centre (Fig. 4b) revealed a sharp contrast of two sets of nearly parallel lines, which is analogous to the morphology of dislocation boundaries seen in Fig. 4a. These features are dislocation slip bands (DSBs) formed during the tensile loading.

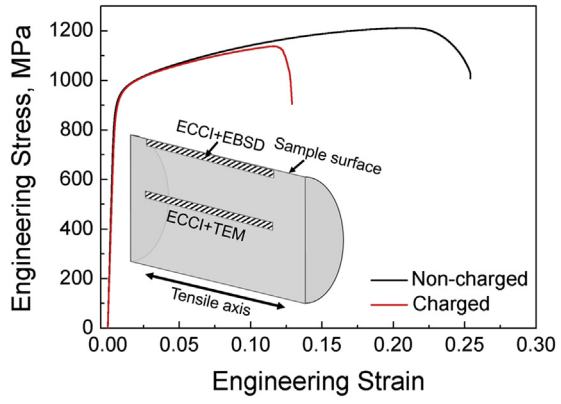

Fig. 2. Engineering tensile stress-strain curves for the Alloy 718 with (red curve) and without (black curve) hydrogen pre-charging. An inset schematic diagram shows the regions, with regard to the longitudinal section of the sample, where post-mortem analysis was carried out. (For interpretation of the references to colour in this figure legend, the reader is referred to the web version of this article.)

The ECC images taken near the specimen outer surface (region with diffused hydrogen) after deformation are shown in Fig. 5. The analysis shows the presence of DSBs similar to those previously described. Interestingly, at the intersections of the two sets of DSBs, a high contrast indicates the presence of defects or nano-voids (see Fig. 5b). However, these features are not present in the region where hydrogen was absent (see Fig. 4b). Therefore, it is hypothesised that the formation of such defects and nano-voids at the intercepting DSBs is associated with hydrogen interfering with the microstructure during straining.

All the above observations, e.g. differences in the microstructure developed during tensioning and the distinct fracture surfaces at regions with and without hydrogen, indicate a change of the failure mode. In order to reveal the failure mechanism of the hydrogen charged region, cracks close to the sample surface were characterised, and four examples are shown in the Fig. 6. A crack with a length of ~25 μm, just beneath the sample surface, can be seen in the ECC image (Fig. 6a). The crack has clearly grown along one set of DSBs of that grain. Fig. 6b shows a crack that deviates its propagation path when it goes into another grain, but is still parallel to the DSBs in the grain. Similarly, Fig. 6c shows a typical example of a crack extending along DSBs, passing through a cracked carbide and then altering its direction when crossing a grain boundary from one set of DSBs to another one. Eventually, Fig. 6d shows a crack encountering a TB: it does not propagate along the TB but, instead, along the DSBs with its path alternating from one set to the other set of DSBs. Without exceptions, all observations demonstrate that cracks prefer to propagate along the DSBs.

Higher magnification ECC images of cracks in the hydrogen-charged region (close to specimen outer surface) are shown in

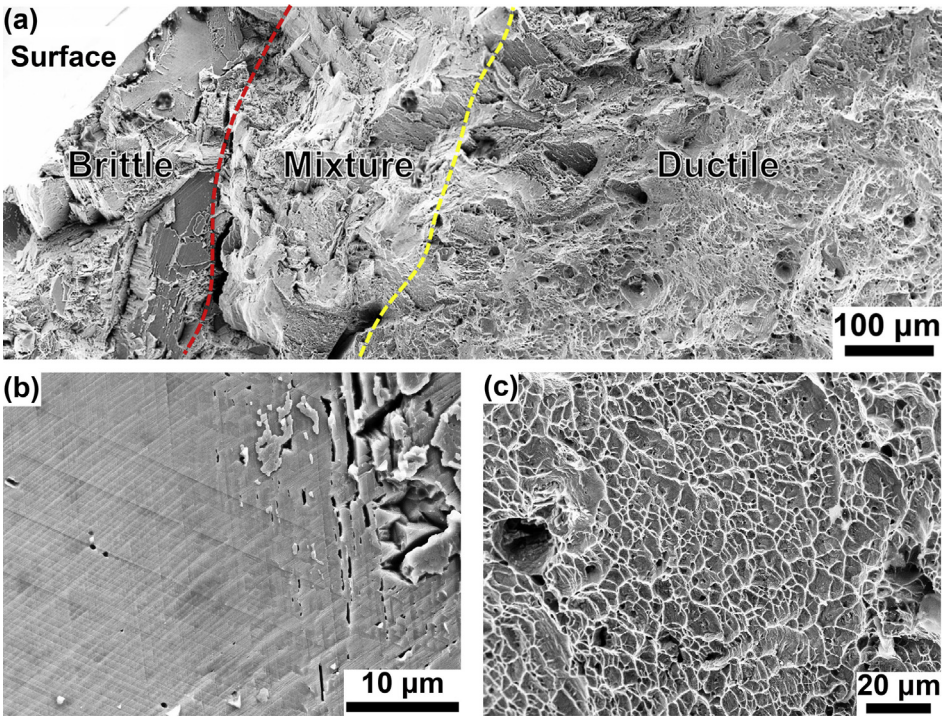

Fig. 3. Images obtained by SEM of the fracture surface of hydrogen pre-charged Alloy 718 tensile specimen after tension to failure: (a) an overview of the fracture surface showing the brittle, transition from brittle to ductile, and ductile failure characters, delimited by dash lines; high resolution fractograph from the brittle (b) failure and ductile(c) failure regions.

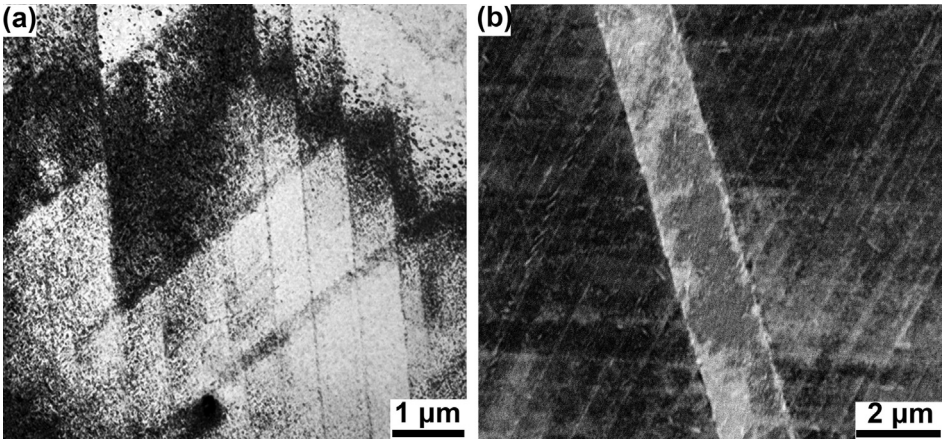

Fig. 4. Microstructure of Alloy 718 after tension from the region where hydrogen had not diffused: (a) TEM and (b) ECC images.

the Fig. 7. Besides a main straight crack, some submicron voids can also be observed aligned with DSBs, especially at their intersecting regions between nonparallel DSBs sets (see Fig. 7a), which is consistent with for example Fig. 5b. Fig. 7b shows a transgranular crack and the subsequent propagation path: the presence of micro-voids, aligned with the DSBs, in proximity of the crack tip is evident and, furthermore, crack progression seems to be the consequence of the coalescence of such micro-voids.

An ECC image in Fig. 8a shows a crack close to the sample surface with a length of ~85 μm. The crack is not completely flat but displays some steps, as shown in Fig. 8b. These steps appear to be aligned with the second set of visible DSBs, intersecting the one parallel to the crack path, as noted in the image by dash lines. A further magnified image, Fig. 8c, from the region near to the crack tip, shows an undulating propagation path with the concave-convex features coinciding with the second set of DSBs, which are nearly perpendicular to the primary crack leading DSBs. This morphology indicates that the intersections of DSBs appear to be weak sites for cracking and cracking is caused by the separation of the upper and lower ridges at these locations.

More detailed analysis on the fracture surface was conducted to reveal the cracking behaviour of Alloy 718 due to hydrogen adsorption. Typical high-resolution SEM fractographic images from the embrittled failure region (close to the sample outer surface) are shown in Fig. 9. It is evident that two or three sets of parallel linear features form on the fracture surface in all cases, which are highly analogous to the DSBs observed in the ECC images (see Figs. 4 and 5). Cracks and micro- and nano-voids can be observed along the

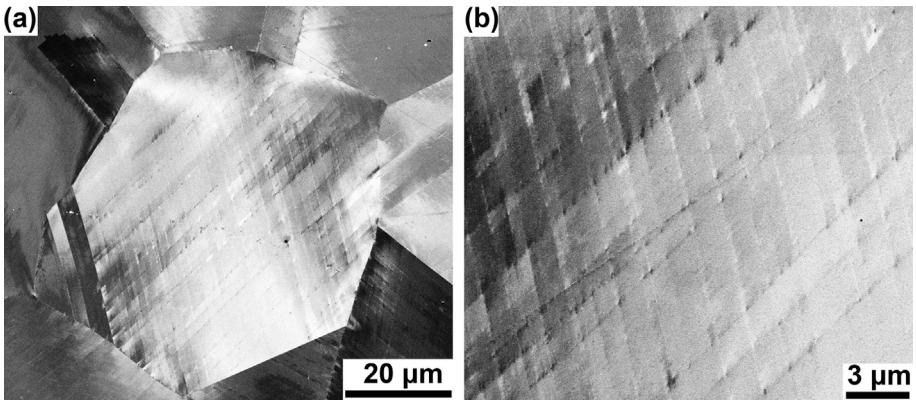

Fig. 5. ECC images of Alloy 718 after tension at the region where hydrogen had the time to diffuse: (a) overview of a grain, and (b) a magnified image from (a).

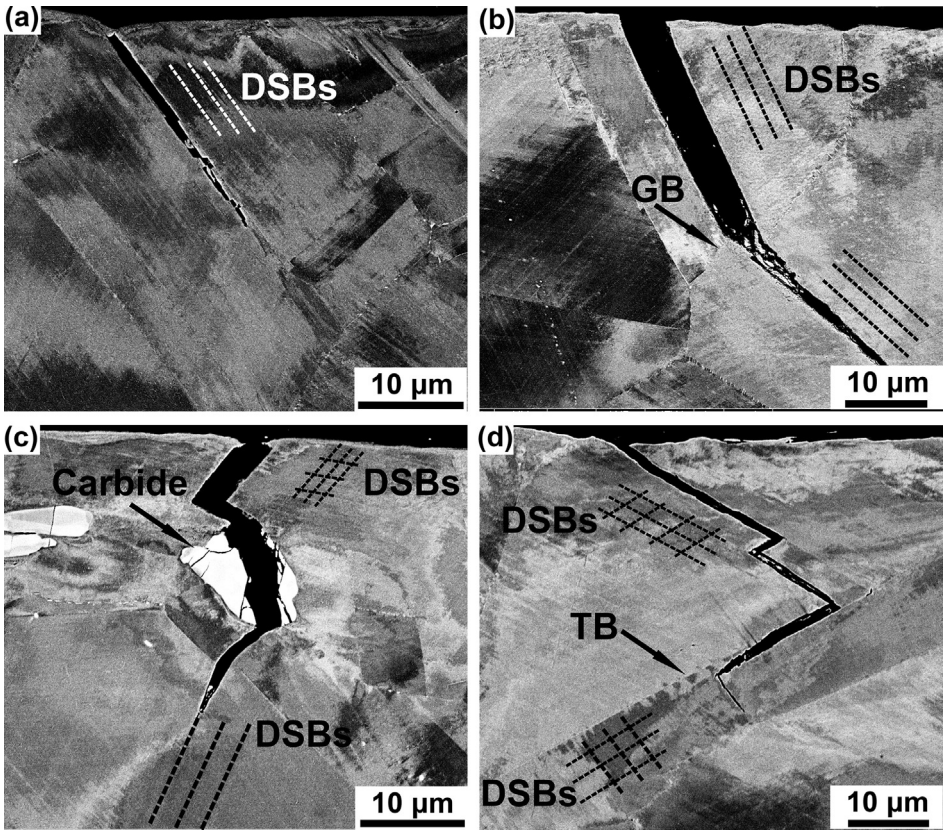

Fig. 6. ECC images from regions close to sample outer surface (top of each image), where hydrogen had the time to diffuse. Visible dislocation slip bands (DSBs), are indicated by dash lines, and some grain boundary (GB) and twin boundary (TB) are noted.

traces, especially at the intersections of nonparallel traces, as seen in Fig. 9b, c. Potential linkage of the voids on the traces can lead to the crack initiation and promote the crack propagation. All these results are phenomenologically consistent with those previous observations in regard to cracking along DSBs revealed by ECCI (see Figs. 5b and 7). Fig. 9d shows knife-edge features formed along the traces, which indicates the final separation along them.

As the microstructure of Alloy 718 contains a high volume fraction of annealing twins (Fig. 1a), the effect of twins on the crack propagation was studied. The interaction between a crack and a series of TBs close to the sample outer surface, i.e. where hydrogen had diffused to, is shown in the ECC images in Fig. 10. The crack propagates following a zigzag path, and it changes its direction when crossing a TB and turns back to the initial direction when leaving the twin (see Fig. 10a,b). Consistently, the crack propagates along the DSBs and never along the TBs. Submicron cracks are also frequently observed on the DSBs (see Fig. 10c) representing possible initiation sites for crack formation and propagation. Furthermore, Fig. 10d clearly shows the presence of γ' but no direct relationship between the crack path and γ' can be observed.

The alternating cracking path between the twins and matrix originates from the mirror relation of dislocation slip planes across the TBs. Dislocation boundaries formed during straining of Alloy 718 also have this relationship, which is illustrated in the TEM image of Fig. 11. In principle, a crack should alternate its path in-between the twin and matrix if it propagates along DSBs. Fig. 12

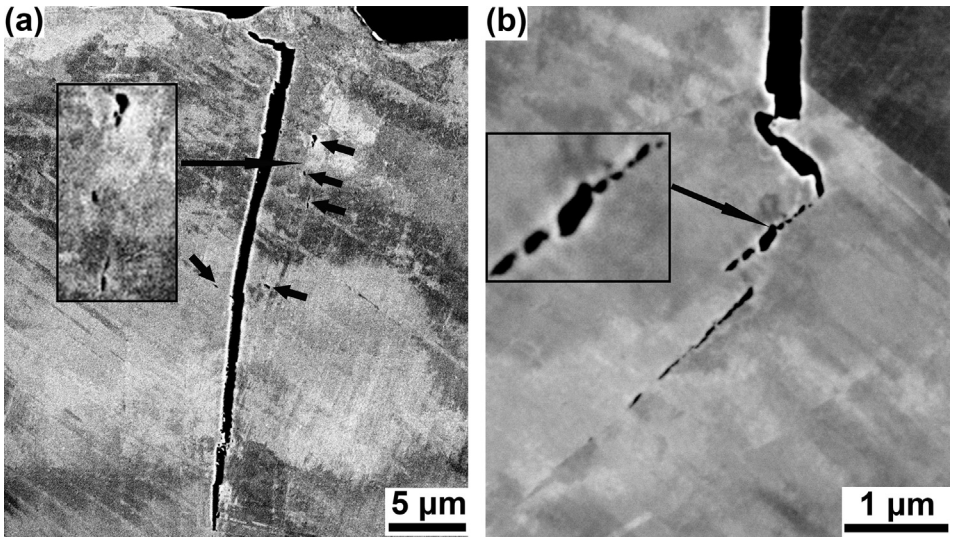

Fig. 7. ECC images from regions close to sample outer surface (where hydrogen had the time to diffuse): (a) a crack and several voids observed at the intersecting regions of DSBs; (b) crack propagation promoted by micro-voids coalescence along DSBs.

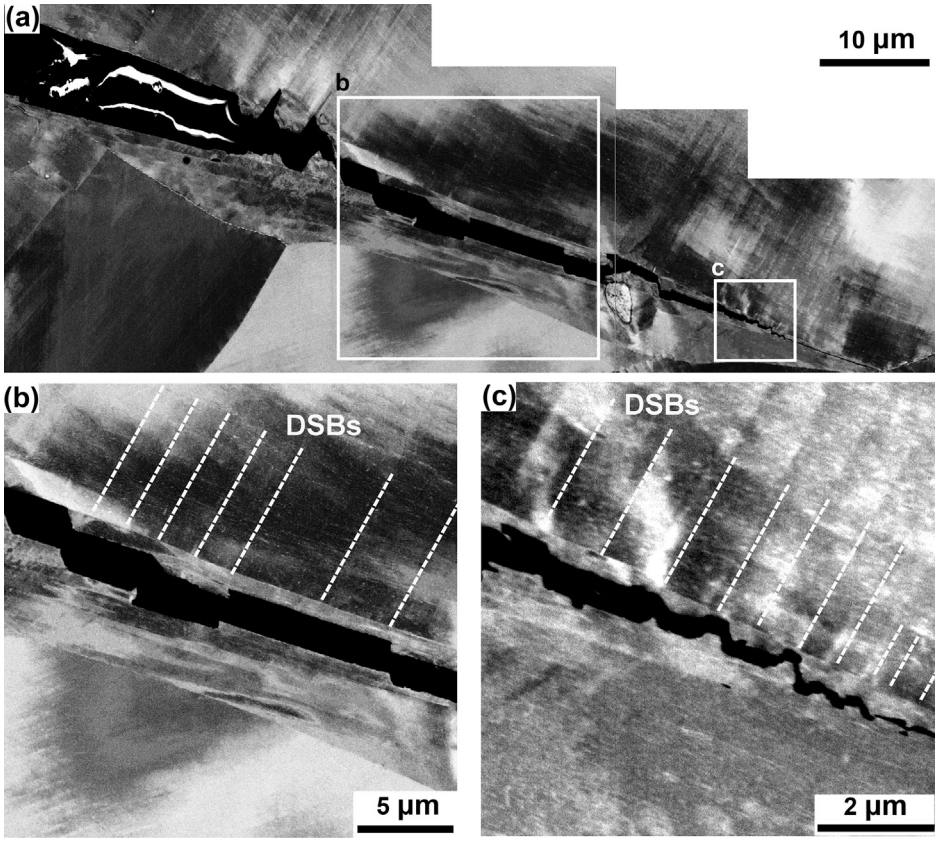

Fig. 8. ECC images showing a crack close to sample outer surface: (a) an overview of the crack; (b) and (c) are magnified images showing more details about the crack in (a). DSBs are indicated by dash lines.

displays a SEM image of the fracture surface from the region where hydrogen and several TBs are present. Similar to the observations in Fig. 9, plenty of micro- and nano-voids formed along the traces but never along TBs. Interestingly, the arrangement of the voids consistently follows the traces in both the matrix and twins, which would facilitate the crack propagation along the traces instead of TBs. This is perfectly consistent with the crack path shown in Fig. 10.

4. Discussion

4.1. Localised dislocation slip and crack initiation

The evidence presented here clearly indicates that crack initiation and propagation are closely associated with planar dislocation slip bands formed during tensioning of Alloy 718 in the presence of

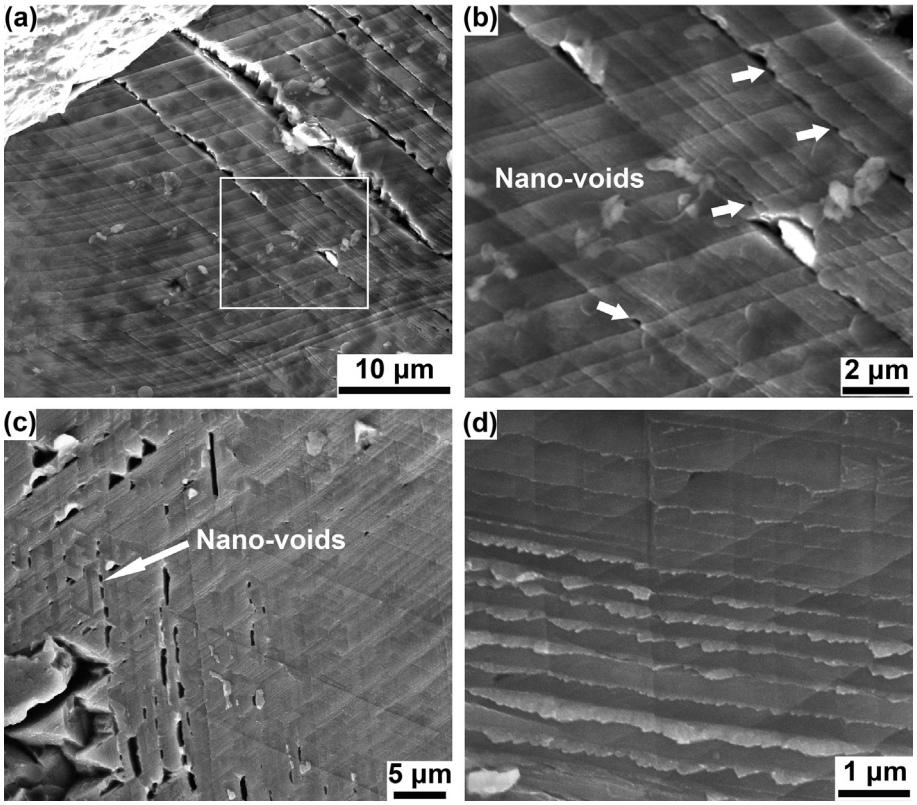

Fig. 9. Fractographs obtained by SEM from the region with hydrogen in presence: (a) image showing the DSBs-like features on the fracture surface; (b) a magnified image from (a) showing the nano-voids formed along the traces; (c) image showing the nano-voids along the traces and potential coalescence to form cracks; (d) image showing saw-teeth shaped features along the traces.

hydrogen. These dislocation boundaries are well aligned with the specific dislocation slip planes, i.e. the {111} crystallographic planes of γ. It is well established that in γ′/γ″ strengthened nickel-based superalloys, the shearing of these precipitates by weakly or strongly coupled dislocation pairs causes the weakening of these slip planes, and thus promotes the slip localisation on the primary slip plane of {111}γ [39–42]. Besides, the addition of high levels of solution elements lowers the stacking fault energy (SFE) in these alloys, which further enhances the dislocation slip planarity. Therefore, in contrast to pure metals, with medium to high stacking fault energy, where low strains result in the formation of a dislocation cell and cell-block structure [43–45], planar dislocation slip bands along {111}γ are the key features of Alloy 718 after plastic deformation [41,42], and these have also been observed in the present study (Fig. 4a). To provide a more detailed image of the dislocation structure, additional dark field TEM analysis was carried out in the hydrogen-charged region of the deformed material. Fig. 13 shows lines of high dislocation density with sparse dislocation debris in-between, which form the planar dislocation boundaries seen by ECCI. It should be mentioned that no appreciable difference in terms of the distance between dislocations was observed in the regions with and without hydrogen, which is probably because the sample had been highly strained.

In addition to the intrinsic plasticity characteristics of Alloy 718, absorption of hydrogen into the materials is supposed to change the dislocation behaviour to some extent. According to the HELP mechanism [18,19], hydrogen can enhance the mobility of dislocations and reduce the barrier for dislocation interaction, thereby promoting slip localisation on the primary slip planes. It has also been reported that hydrogen uptake reduces the SFE of materials and hence hinders dislocation cross slip [46], which results in further constrain on dislocation slip away from the initial slip plane during the self-arrangement process.

In summary, both the intrinsic character of Alloy 718 and the externally imposed effect from hydrogen contribute to the process: dislocation slip localisation on {111} crystallographic planes and formation of dislocation boundaries on the initial slip planes. Since dislocations are able to transport hydrogen during plastic deformation [47,48], these planes with extensive dislocation slip and high dislocation density are believed to contain higher concentration of hydrogen. Interaction between dislocations and hydrogen tends to make these planes more susceptible to crack initiation and propagation [9].

4.2. Linkage of crack initiation and propagation

Micro-voids coalescence is thought to be the dominant mechanism for the formation of dimples in a ductile fracture [49]. The quasi-cleavage fracture of hydrogen embrittled Alloy 718 suggests a different process in crack initiation and propagation due to the presence of hydrogen. Besides the ECCI analysis on the cracks near the sample surface (Figs. 6–9), more detailed fractographs from the quasi-cleavage regions provide additional insight on the hydrogen induced cracking in Alloy 718 (Fig. 11). Analogous to the DSBs seen in ECCI and TEM analysis, very similar features were observed at the fracture surface close to the sample outer surface, i.e. in the region affected by hydrogen. Since these traces on the fracture surface exhibited high consistency with the DSBs observed in the TEM and ECC images, in terms of morphology and length scale, it is very likely that those features on the fracture surface are correlated with the DSBs. It might be argued that these features also have a similar morphology to the slip traces observed on a sample surface when

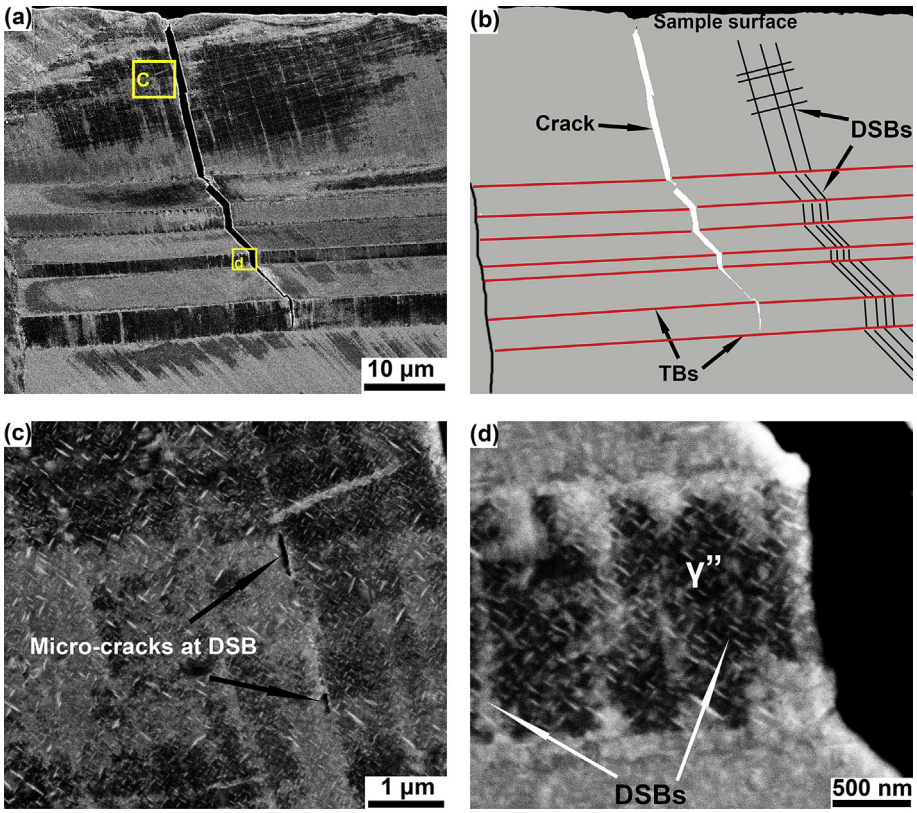

Fig. 10. ECC images showing crack propagation across several twin boundaries (TBs). (a) an overview ECC image and (b) its corresponding schematic, with DSBs and TBs highlighted. (c) and (d) are magnified ECC images from the regions framed in (a) showing more details about micro-cracks at DSBs and finer microstructural features.

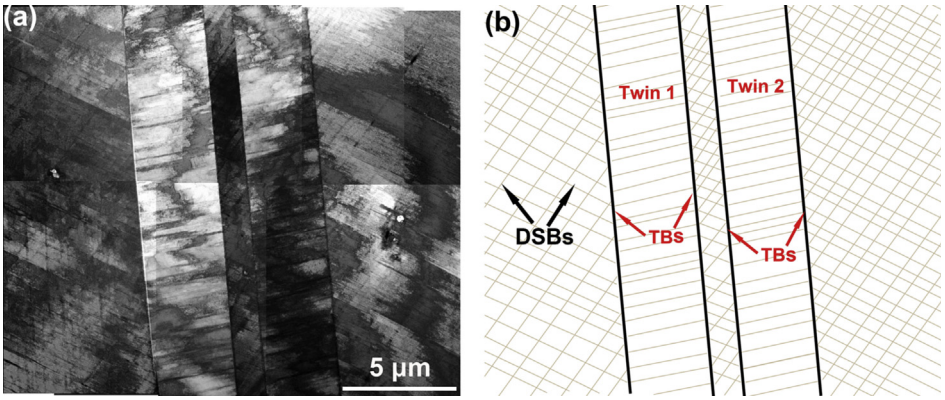

Fig. 11. (a) A TEM image and (b) its corresponding schematic showing the dislocation structures developed during tension in the region with TBs.

the material is plastically deformed [50], however, they are of essential difference, since the traces on the fracture surface can only form during cracking and failure process, instead of during deformation only. In this context, cracking and failure in the hydrogen embrittled region is closely associated with the dislocation slip bands, i.e. cracks tend to initiate and propagate along the dislocation slip bands.

Other researchers have also invoked the concept of failure along the dislocation slip bands in the hydrogen pre-charged materials [11,22,51]. After studying the quasi-cleavage fracture surface and the underneath microstructure, Martin et al. [22] and Neeraj et al. [11] proposed mechanisms for the hydrogen assisted crack initiation and propagation in hydrogen charged steels. Although both mechanisms are within the framework of the HELP mechanism, the detailed claims are quite different. Martin et al. [22] suggested that critical hydrogen concentrations might be achieved in the regions with slip localisation and high density of dislocations, and thus hydrogen at these sites may be sufficiently high to cause a significant reduction in lattice cohesive strength, which facilitates the crack initiation and propagation. In contrast, Neeraj et al. [11] suggested that the interactions between hydrogen and dislocations activities in the localised slip regions promote the nucleation of nano-voids and the linkage of these voids leads to the crack initiation and propagation. Both mechanisms support the phenomenon of cracking along DSBs, however, the conjugate mound-on-mound morphology frequently observed at the crack tip in ECC images (e.g. Fig. 7b) and in fractographs (e.g. Fig. 9b, c) in the present case of Alloy 718 favours the nano-voids coalescence

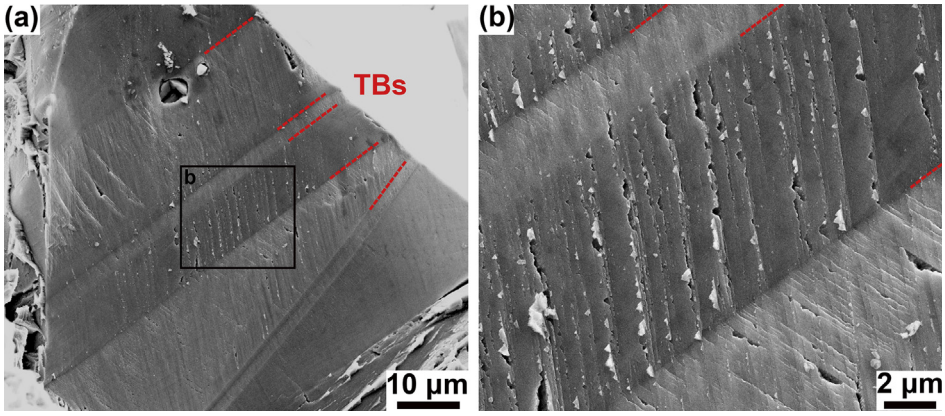

Fig. 12. (a) Fractograph from the region affected by hydrogen diffusion with TBs indicated by red dash lines; (b) a magnified image from the framed region in (a) showing DSBs-like features and micro- and nano-voids along them. (For interpretation of the references to colour in this figure legend, the reader is referred to the web version of this article.)

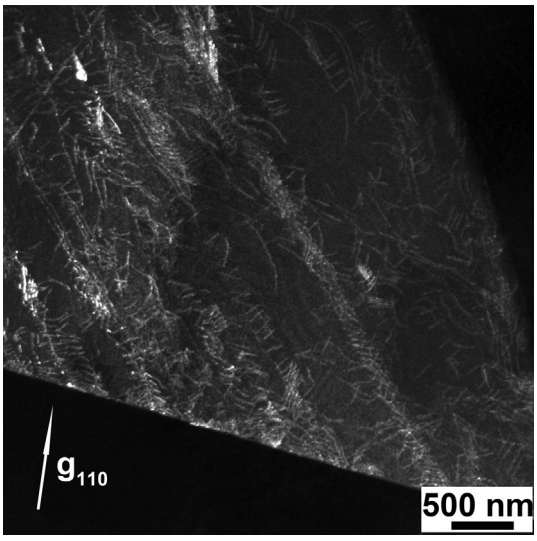

Fig. 13. Dark field TEM image showing the dislocation structure formed during tension.

mechanism. Solid evidence is shown in Figs. 7, 9 and 12, where nanoscale voids form along DSBs, particularly at the intersections of nonparallel DSBs, and void coalescence and widening leads to crack initiation. The arrangement and configuration of the micro- and nano-voids (e.g. Figs. 7b and 9c) implies the formation of valley-on-valley fracture surface. Although relatively smooth and flat cracks could be seen in some cases (Fig. 6) and even a valley-on-mound shape formed at a crack tip (Fig. 8c), these features cannot rule out the possible nano-void coalescence mechanism, since nano-scale voids initiated at a much smaller scale than the observed crack [11]. It is worth noting that hydrogen-associated cracking in ferritic steels [11,22,51] is usually not of such localised nature as in the present case. However, studying hydrogen embrittlement in a precipitation strengthened austenitic steel with yield strength up to 1 GPa, Koyama et al. [32] observed slip localisation and fracture surfaces which were similar to the present work. However, their work indicated that voids tend to nucleate at the triple junctions of grain boundaries and at intersecting sites between the dislocation slip planes and grain boundaries, which was not observed in the present study. The reason could be that cracking along grain boundaries is an intrinsic character of such high strength steel, as pointed out by the authors, and the presence of hydrogen only exasperates this effect.

Since nano-voids can form by vacancy agglomeration, on which hydrogen would probably exert influence, crack initiation by nano-voids preferentially occurs along dislocation boundaries in presence of hydrogen [52]. It is well documented that vacancies can be generated in materials during plastic deformation by dislocation activities [53]. These vacancies are thought to be instable but gaseous impurities like oxygen and hydrogen are known to stabilize them [54]. Indeed, atomic simulations suggest that hydrogen is able to stabilize vacancies by formation of a hydrogen-vacancy complex, which can act as an embryo for void formation [29,55]. Therefore, dislocations slip bands, such as those observed here in Alloy 718, naturally become potential locations for void nucleation in the presence of hydrogen. Such potential is enhanced at dislocation slip band intersections, due to higher concentrations of hydrogen and more extensive dislocation slip.

Consequently, hydrogen-induced cracking along DSBs in Alloy 718 leads to quasi-cleavage failure mode and formation of transgranular fracture surface. While hydrogen is much well known to cause intergranular failure, involving crack initiation and propagation along grain boundaries in many metals and alloys [24,27,57,58], hydrogen-induced transgranular fracture was also reported in precipitation strengthened nickel-based superalloys [3,5,56]. Recent studies have provided new insight on hydrogen-enhanced dislocation activities establishing conditions that promote intergranular failure [24,27]. Thus it seems that hydrogen-induced transgranular and intergranular fracture involve a common process, namely enhanced dislocation activity by hydrogen. The major difference between Alloy 718 and other materials showing intergranular failure is the enhanced slip localisation in Alloy 718 due to the high volume fraction of nano-sized precipitates and the low SFE. Such pronounced slip localisation and the simultaneous dislocation and hydrogen interaction promote dislocation slip planes becoming the most susceptible sites for the crack initiation and propagation rather than the grain boundaries. In the nickel-based superalloy with solid solution strengthening, where slip localisation is supposed to be lower than Alloy 718, hydrogen-induced intergranular cracking was found to be dominant with transgranular fracture only in some occasions [3]. In addition, precipitates and segregates on grain boundaries tend to incur intergranular cracking in the materials with hydrogen present [57,58]. In a study on the hydrogen embrittlement of Alloy 718 with carbides and δ phase decorated grain boundaries, cracks were occasionally found along boundaries with those precipitates [59]. Since microscopically ductile features were observed in the vicinity of these boundaries, it suggests that slip localisation, which

interacts with precipitates at grain boundaries, causes void formation along grain boundaries with hydrogen present. It should be noted that cracking along DSBs and altering the crack paths at grain boundaries lead to the formation of a fracture surface similar to intergranular failure.

4.3. Role of twin boundaries on hydrogen induced cracking

Annealing twins are common microstructural features in nickel-based superalloys such as Alloy 718, as seen in Fig. 1a. In terms of hydrogen-induced embrittlement, TBs are thought to be less vulnerable, since TBs are known to have high separation energy and low hydrogen solubility [60,61]. Recent work by Seita et al. [6] proposed a dual role of TBs in the hydrogen embrittlement of Inconel 725, namely the TBs are most susceptible to crack initiation but with higher resistance to crack propagation. However, in the present study, neither void formation nor crack initiation and propagation were found to be associated with TBs. Examples shown in Figs. 6d and 9 demonstrated that cracks prefer to propagate along the DSBs even though the DSBs only have a small inclined angle to the TB (Fig. 6d), or even though this requires significant changes of the crack path (Fig. 9). The result from Fig. 12 can underpin and interpret such phenomenon very well, since many voids and cracks formed along DSBs but no void initiation was observed along the TBs. Further analysis on the orientation of the crack propagation path across TBs demonstrates that the crack path is always coincided with one specific {111} crystallographic plane (Fig. 14), which is also the plane of DSBs. The Kernel average misorientation map (Fig. 14b) shows DSBs and the crack propagation path are parallel to the lines with higher misorientation gradients. Although strain localisation is observed adjacent to the TBs, cracks seldom propagate along them. Therefore, it indicates that strain localisation on its own is not the root cause for hydrogen-induced cracking, and it is the dislocation slip localisation interplaying with hydrogen that promote the crack initiation and propagation.

This discrepancy between the present work and the work reported by Seita et al. [4] may be attributed to several factors, including the slight difference in the material chemistry, different pre-charging conditions, different test conditions, etc. The most important reason is likely to be the considerable difference in the strain rate of the tensile test. The strain rate used in Ref. [4] was 100 times higher (10^{-4} s^{-1}) than that used in the present study (10^{-6} s^{-1}). Since dislocation motion and interaction with hydrogen will inevitably be highly strain rate sensitive, these processes are expected to be less pronounced when the sample is tested at high strain rate. Therefore, it is reasonable that cracking along dislocation slip bands, originated from the strong interaction between dislocation and hydrogen, does not take effect at strain rates of 10^{-4} s^{-1}. Further systematic studies about the strain rate effect on the hydrogen induced cracking behaviour of nickel-based superalloys will be carried out in the near future to elucidate this aspect.

4.4. Summary of hydrogen assisted cracking mechanism in Alloy 718

All experimental results presented here demonstrate a direct relationship between dislocation slip localisation and hydrogen assisted cracking in Alloy 718. Accordingly, an envisioned mechanism of hydrogen-induced embrittlement of Alloy 718 is proposed, which is summarized schematically in Fig. 15. Once the alloy is strained beyond yielding, dislocation generation and multiplication commence. Due to microstructural (γ' and γ'') and alloy chemistry effects (low SFE), planar dislocation slip leads to the formation of planar dislocation slip bands, Fig. 15b. In the presence of hydrogen (here <200 μm beneath the surface), slip planarity and localisation is suggested to be further promoted within the framework of the HELP mechanism [18–20,46]. It has been demonstrated that dislocations are capable of transporting hydrogen at low strain rates [47,48] and dislocations can act as trapping sites for hydrogen [62]. Therefore high concentrations of hydrogen agglomerate at dislocation slip bands, especially at their intersections (Fig. 15c). Consequently, extensive hydrogen-dislocation interaction at these sites leads to the formation of nano-voids. Nano-voids weaken the dislocation boundaries and their subsequent widening and coalescence via dislocation process results in crack initiation and propagation along the dislocation boundaries (Fig. 15d). It should be mentioned that in the present study the effect of γ'' precipitates on the hydrogen embrittlement is only in respect to the promotion of slip localisation and constrain of dislocation cross slip. The detailed microstructural analysis did not provide any evidence for decohesion along the γ/γ'' interface, despite such interface potentially being the trapping site for hydrogen. Future work employing nanoscale secondary ion mass spectrometry will be carried out to

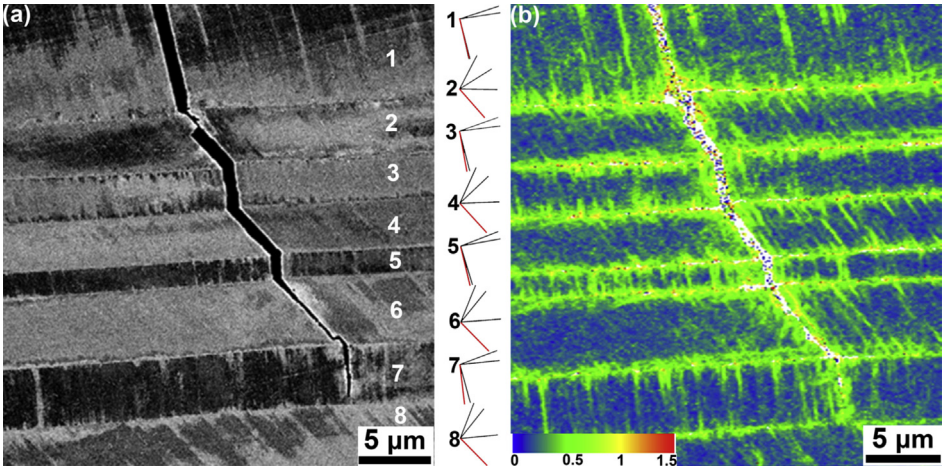

Fig. 14. (a) An ECC image and (b) a Kernel average misorientation (KAM) map obtained from the EBSD data from the same area. The {111} crystallographic plane traces of the numbered regions are indicated in the middle, with the ones parallel to the crack paths colored in red. (For interpretation of the references to colour in this figure legend, the reader is referred to the web version of this article.)

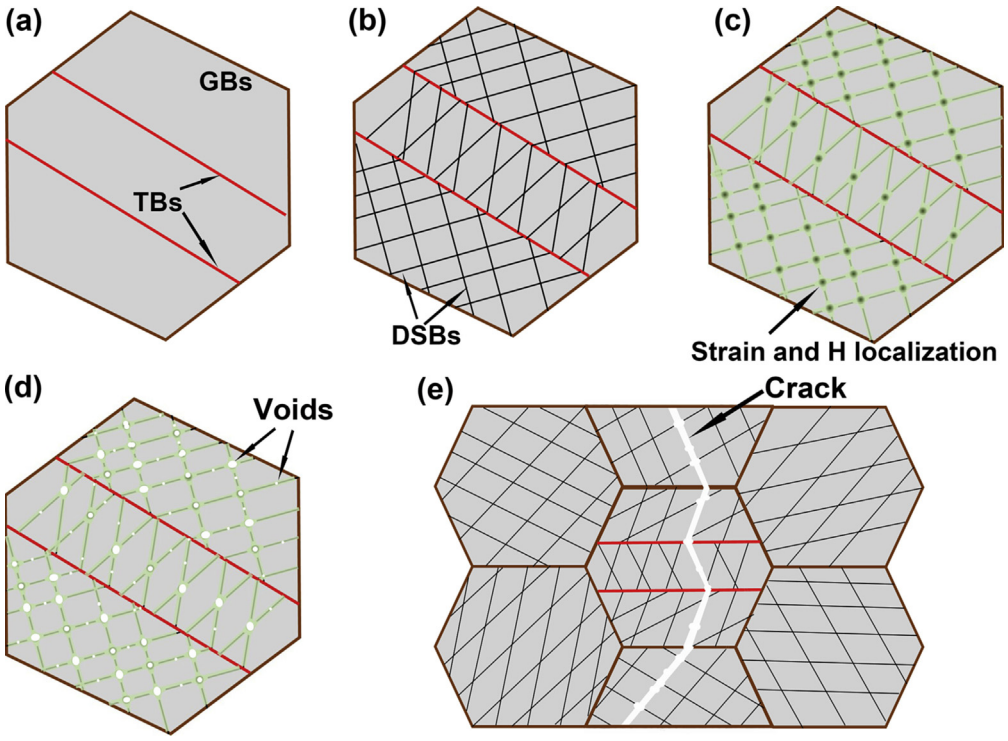

Fig. 15. Schematic diagrams showing the envisaged mechanism for the hydrogen induced crack initiation and propagation in Alloy 718: (a) material prior to deformation; (b) planar dislocation slip bands (DSBs) develop during tensioning; (c) on the DSBsand in particular the intersections of DSBs, slip localisation is more intensive and concentration of hydrogen is supposed to be high; (d) higher concentration hydrogen and localised slip promote the nucleation of nanoscale voids; (e) coalescence and widening of voids via dislocation process leads to crack propagation along the DSBs.

relate preferential hydrogen sites to microstructural features, including precipitates and dislocation slip bands.

5. Conclusions

Hydrogen induced embrittlement in hydrogen charged Alloy 718 slowly strained to failure was investigated by means of detailed electron microscopy in order to develop a better mechanistic understanding of crack initiation and propagation. Observations within the hydrogen charged region were compared with the non-hydrogen charged region. The main findings can be summarized as follows:

1) Hydrogen charging results in significant reduction in the tensile ductility of Alloy 718, with quasi-cleavage fracture in the region with hydrogen present.
2) The deformation microstructure of Alloy 718 developed during slow strain rate tensioning to failure is characterised by considerable slip localisation and formation of planar dislocation slip bands along the {111}γ planes in the non-hydrogen charged and hydrogen charged regions.
3) In the hydrogen charged region, cracks form along the planar dislocation slip bands, and this leads to the formation of slip-traces like features on the fracture surface, whereas cracking along grain boundaries and twin boundaries was not observed.
4) Nucleation of nano-voids along dislocation slip bands, particularly at intersections of differently orientated dislocation slip bands resulting from the interaction between dislocation slip localisation and probably hydrogen agglomeration, leads to cracking along these planes. Coalescence and widening of the voids via dislocation process promotes the crack initiation and propagation.

Acknowledgement

The authors would like to acknowledge the funding and technical support from BP through the BP International Centre for Advanced Materials (BP-ICAM), which made this research possible. We would like to thank Dr Viviane Smith and Dr John Martin for extensive discussions and Dr Octav Ciuca for the initial training and help on the FEI Magellan microscope.

References

[1] T.E. Perez, Corrosion in the oil and gas industry: an increasing challenge for materials, JOM 65 (2013) 1033–1042.
[2] G. DeBrujin, C. Skeates, R. Greenaway, D. Harrison, M. Parris, S. James, F. Mueller, S. Ray, M. Riding, L. Temple, K. Wutherich, High-pressure, high-temperature technologies, Oilfield Rev. 20 (2008) 46–60.
[3] P.D. Hicks, C.J. Altstetter, Hydrogen-enhanced cracking of superalloys, Metall. Trans. A 23 (1992) 237–249.
[4] F. Galliano, E. Andrieu, C. Blanc, J.M. Cloue, D. Connetable, G. Odemer, Effect of trapping and temperature on the hydrogen embrittlement susceptibility of alloy 718, Mater. Sci. Eng. A 611 (2014) 370–382.
[5] L.F. Liu, C.Q. Zhai, C. Lu, W.J. Ding, A. Hirose, K.F. Kobayashi, Study of the effect of delta phase on hydrogen embrittlement of Inconel 718 by notch tensile tests, Corros. Sci. 47 (2005) 355–367.
[6] M. Seita, J.P. Hanson, S. Gradecak, M.J. Demkowicz, The dual role of coherent twin boundaries in hydrogen embrittlement, Nat. Commun. 6 (2015).
[7] D.G. Westlake, The habit planes of zirconium hydride in zirconium and zircaloy, J. Nucl. Mater 26 (1968) 208–216.
[8] C.D. Beachem, New model for hydrogen-assisted cracking (hydrogen embrittlement), Metall. Trans. 3 (1972) 437–451.
[9] I.M. Robertson, H.K. Birnbaum, An HVEM study of hydrogen effects on the deformation and fracture of nickel, Acta Metall. 34 (1986) 353–366.
[10] M. Nagumo, Function of hydrogen in embrittlement of high-strength steels, ISIJ Int. 41 (2001) 590–598.
[11] T. Neeraj, R. Srinivasan, J. Li, Hydrogen embrittlement of ferritic steels: observations on deformation microstructure, nanoscale dimples and failure by nanovoiding, Acta Mater 60 (2012) 5160–5171.
[12] R.A. Oriani, Whitney award lecture 1987-hydrogen - the versatile embrittler, Corrosion 43 (1987) 390–397.

[13] R.A. Oriani, P.H. Josephic, Hydrogen-enhanced load relaxation in a deformed medium-carbon steel, Acta Metall. 27 (1979) 997–1005.
[14] D. Tromans, On surface-energy and the hydrogen embrittlement of iron and steels, Acta Metall. Mater 42 (1994) 2043–2049.
[15] W.T. Geng, A.J. Freeman, R. Wu, C.B. Geller, J.E. Raynolds, Embrittling and strengthening effects of hydrogen, boron, and phosphorus on a Sigma 5 nickel grain boundary, Phys. Rev. B 60 (1999) 7149–7155.
[16] Y.A. Du, L. Ismer, J. Rogal, T. Hickel, J. Neugebauer, R. Drautz, First-principles study on the interaction of H interstitials with grain boundaries in α- and γ-Fe, Phys. Rev. B 84 (2011) 144121.
[17] S.E. Kulkova, S.S. Kulkov, A.V. Bakulin, S. Hocker, S. Schmauder, First-principles study of the hydrogen absorption at Σ5 symmetrical tilt grain boundary in B2-TiFe alloy, Int. J. Hydrogen Energy 37 (2012) 6666–6673.
[18] P. Sofronis, H.K. Birnbaum, Mechanics of the hydrogen-dislocation-impurity interactions .1. increasing shear modulus, J. Mech. Phys. Solids 43 (1995) 49–90.
[19] I.M. Robertson, H.K. Birnbaum, P. Sofronis, Hydrogen effects on plasticity, Dislocations Solids 15 (15) (2009) 249–293.
[20] P.J. Ferreira, I.M. Robertson, H.K. Birnbaum, Hydrogen effects on the interaction between dislocations, Acta Mater 46 (1998) 1749–1757.
[21] J.P. Chateau, D. Delafosse, T. Magnin, Numerical simulations of hydrogen-dislocation interactions in fcc stainless steels. Part 1: hydrogen-dislocation interactions in bulk crystals, Acta Mater 50 (2002) 1507–1522.
[22] M.L. Martin, J.A. Fenske, G.S. Liu, P. Sofronis, I.M. Robertson, On the formation and nature of quasi-cleavage fracture surfaces in hydrogen embrittled steels, Acta Mater 59 (2011) 1601–1606.
[23] M.L. Martin, I.M. Robertson, P. Sofronis, Interpreting hydrogen-induced fracture surfaces in terms of deformation processes: a new approach, Acta Mater 59 (2011) 3680–3687.
[24] M.L. Martin, B.P. Somerday, R.O. Ritchie, P. Sofronis, I.M. Robertson, Hydrogen-induced intergranular failure in nickel revisited, Acta Mater 60 (2012) 2739–2745.
[25] A. Nagao, M.L. Martin, M. Dadfarnia, P. Sofronis, I.M. Robertson, The effect of nanosized (Ti,Mo)C precipitates on hydrogen embrittlement of tempered lath martensitic steel, Acta Mater 74 (2014) 244–254.
[26] A. Nagao, C.D. Smith, M. Dadfarnia, P. Sofronis, I.M. Robertson, The role of hydrogen in hydrogen embrittlement fracture of lath martensitic steel, Acta Mater 60 (2012) 5182–5189.
[27] S. Wang, M.L. Martin, P. Sofronis, S. Ohnuki, N. Hashimoto, I.M. Robertson, Hydrogen-induced intergranular failure of iron, Acta Mater 69 (2014) 275–282.
[28] I.M. Robertson, P. Sofronis, A. Nagao, M.L. Martin, S. Wang, D.W. Gross, K.E. Nygren, Hydrogen embrittlement understood, Metall. Mater. Trans. B 46 (2015) 1085–1103.
[29] S. Li, Y. Li, Y.-C. Lo, T. Neeraj, R. Srinivasan, X. Ding, J. Sun, L. Qi, P. Gumbsch, J. Li, The interaction of dislocations and hydrogen-vacancy complexes and its importance for deformation-induced proto nano-voids formation in α-Fe, Int. J. Plast. 74 (2015) 175–191.
[30] I.M. Robertson, H.K. Birnbaum, Effect of hydrogen on the dislocation-structure of deformed nickel, Scr. Metall. 18 (1984) 269–274.
[31] M. Koyama, C.C. Tasan, E. Akiyama, K. Tsuzaki, D. Raabe, Hydrogen-assisted decohesion and localized plasticity in dual-phase steel, Acta Mater 70 (2014) 174–187.
[32] M. Koyama, H. Springer, S.V. Merzlikin, K. Tsuzaki, E. Akiyama, D. Raabe, Hydrogen embrittlement associated with strain localization in a precipitation-hardened Fe-Mn-Al-C light weight austenitic steel, Int. J. Hydrogen Energy 39 (2014) 4634–4646.
[33] M. Koyama, E. Akiyama, K. Tsuzaki, D. Raabe, Hydrogen-assisted failure in a twinning-induced plasticity steel studied under in situ hydrogen charging by electron channeling contrast imaging, Acta Mater 61 (2013) 4607–4618.
[34] R.J. Walter, W.T. Chandler, Influence of hydrogen pressure and notch severity on hydrogen-environment embrittlement at ambient temperatures, Mater. Sci. Eng. 8 (1971) 90–97.
[35] R.J. Walter, R.P. Jewett, W.T. Chandler, On mechanism of hydrogen-environment embrittlement of iron- and nickel-base alloys, Mater. Sci. Eng. 5 (1970) 99–110.
[36] L.F. Liu, L. Chen, C.Q. Zhai, W.J. Ding, A. Hirose, K.F. Kobayashi, Effect of annealing conditions on hydrogen embrittlement of Inconel 718, Rare Metal. Mater. Eng. 34 (2005) 954–958.
[37] L.F. Liu, C. Lu, W.J. Ding, A. Hirose, K.F. Kobayashi, Effect of delta phase on hydrogen embrittlement of inconel 718 by notch tensile tests, J. Mater. Sci. Technol. 21 (2005) 256–260.
[38] J. Xu, X.K. Sun, Q.Q. Liu, W.X. Chen, Hydrogen permeation behavior in IN718 and GH761 superalloys, Metall. Mater. Trans. A 25 (1994) 539–544.
[39] H.F. Merrick, Effect of heat-treatment on structure and properties of extruded P-M Alloy 718, Metall. Trans. A 7 (1976) 505–514.
[40] J.M. Oblak, D.F. Paulonis, D.S. Duvall, Coherency strengthening in ni base alloys hardened by Do22 gamma' precipitates, Metall. Trans. 5 (1974) 143–153.
[41] L. Xiao, D.L. Chen, M.C. Chaturvedi, Shearing of gamma' precipitates and formation of planar slip bands in Inconel 718 during cyclic deformation, Scr. Mater 52 (2005) 603–607.
[42] M. Sundararaman, P. Mukhopadhyay, S. Banerjee, Deformation-behavior of gamma' strengthened Inconel-718, Acta Metall. 36 (1988) 847–864.
[43] D.A. Hughes, N. Hansen, Microstructural evolution in nickel during rolling from intermediate to large strains, Metall. Trans. A 24 (1993) 2021–2037.
[44] Q. Liu, X. Huang, D.J. Lloyd, N. Hansen, Microstructure and strength of commercial purity aluminium (AA 1200) cold-rolled to large strains, Acta Mater 50 (2002) 3789–3802.
[45] B.L. Li, A. Godfrey, Q.C. Meng, Q. Liu, N. Hansen, Microstructural evolution of IF-steel during cold rolling, Acta Mater 52 (2004) 1069–1081.
[46] A.E. Pontini, J.D. Hermida, X-Ray diffraction measurement of the stacking fault energy reduction induced by hydrogen in an AISI 304 steel, Scr. Mater 37 (1997) 1831–1837.
[47] G.S. Frankel, R.M. Latanision, Hydrogen transport during deformation in nickel .1. polycrystalline nickel, Metall. Trans. A 17 (1986) 861–867.
[48] M. Dadfarnia, M.L. Martin, A. Nagao, P. Sofronis, I.M. Robertson, Modeling hydrogen transport by dislocations, J. Mech. Phys. Solids 78 (2015) 511–525.
[49] D. Hull, Fractography: Observing, Measuring and Interpreting Fracture Surface Topography, Cambridge University Press, 1999.
[50] F. Di Gioacchino, J. Quinta da Fonseca, An experimental study of the polycrystalline plasticity of austenitic stainless steel, Inter. J. Plast. 74 (2015) 92–109.
[51] K.A. Nibur, B.P. Somerday, D.K. Balch, C. San Marchi, The role of localized deformation in hydrogen-assisted crack propagation in 21Cr-6Ni-9Mn stainless steel, Acta Mater 57 (2009) 3795–3809.
[52] R. Kirchheim, B. Somerday, P. Sofronis, Chemomechanical effects on the separation of interfaces occurring during fracture with emphasis on the hydrogen-iron and hydrogen-nickel system, Acta Mater 99 (2015) 87–98.
[53] A. Seeger, The generation of lattice defects by moving dislocations, and its application to the temperature dependence of the flow-stress of FCC crystals, Philos. Mag. 46 (1955) 1194–1217.
[54] S.J. Zinkle, W.G. Wolfer, G.L. Kulcinski, L.E. Seitzman, Stability of vacancy clusters in metals .2. effect of oxygen and helium on void formation in metals, Philos. Mag. A 55 (1987) 127–140.
[55] Y. Tateyama, T. Ohno, Stability and clusterization of hydrogen-vacancy complexes in α-Fe: an ab initio study, Phys. Rev. B 67 (2003) 174105.
[56] S.S. Shademan, J.W. Martin, A.P. Davis, UNS N07725 Nickel Alloy Connection Failure, NACE International, 2012.
[57] C.J. McMahon, Hydrogen-induced intergranular fracture of steels, Eng. Fract. Mech. 68 (2001) 773–788.
[58] P. Novak, R. Yuan, B.P. Somerday, P. Sofronis, R.O. Ritchie, A statistical, physical-based, micro-mechanical model of hydrogen-induced intergranular fracture in steel, J. Mech. Phys. Solids 58 (2010) 206–226.
[59] T. Cassagne, M. Bonis, D. Hills, C. Duret, Understanding field failures of alloy 718 forging materials in HP/HT wells, in: E.V. Dechema (Ed.), EUROCORR, European Corrosion Congress, Frankfurt, 2008.
[60] V. Randle, Twinning-related grain boundary engineering, Acta Mater 52 (2004) 4067–4081.
[61] G. Palumbo, K.T. Aust, Solute effects in grain-boundary engineering, Can. Metall. Q. 34 (1995) 165–173.
[62] A. Pundt, R. Kirchheim, Hydrogen in metals: microstructural aspects, Annu. Rev. Mater. Res. 36 (2006) 555–608.